The Astrophysical Journal, 793:81 (7pp), 2014 October 1 doi:10.1088/0004-637X/793/2/81

POLARIZED MID-INFRARED SYNCHROTRON EMISSION IN THE CORE OF CYGNUS A

E. Lopez-Rodriguez[1], C. Packham[1], C. Tadhunter[2], R. Mason[3], E. Perlman[4], A. Alonso-Herrero[5,13], C. Ramos Almeida[6,7,14], K. Ichikawa[8], N. A. Levenson[9], J. M. Rodríguez-Espinosa[6,7], C. A. Álvarez[7,10], E. A. Ramírez[11], and C. M. Telesco[12]

[1] Department of Physics & Astronomy, University of Texas at San Antonio, One UTSA Circle, San Antonio, TX 78249, USA
[2] Department of Physics & Astronomy, University of Sheffield, Sheffield S3 7RH, UK
[3] Gemini Observatory, Northern Operations Center, 670 North A'ohoku Place, Hilo, HI 96720, USA
[4] Department of Physics and Space Sciences, Florida Institute of Technology, Melbourne, FL 32901, USA
[5] Instituto de Física de Cantabria, CSIC-UC, E-39005 Cantabria, Spain
[6] Instituto de Astrofísica de Canarias, Calle Vía Láctea s/n, E-38205 Tenerife, Spain
[7] Departamento de Astrofísica, Universidad de La Laguna, E-38206 La Laguna, Tenerife, Spain
[8] Department of Astronomy, Graduate School of Science, Kyoto University, Kitashirakawa-Oiwake cho, Kyoto 606-8502, Japan
[9] Gemini Observatory, Casilla 603, La Serena, Chile
[10] GTC Project, Instituto de Astrofísica de Canarias (IAC), E-38200 La Laguna, Tenerife, Spain
[11] Universidade de São Paulo, IAG, Rua do Matão 1226, Cidade Universitária, São Paulo 05508-900, Brazil
[12] Department of Astronomy, University of Florida, 211 Bryant Space Science Center, P.O. Box 11205, Gainesville, FL 32611-2055, USA
Received 2013 December 3; accepted 2014 July 22; published 2014 September 9

ABSTRACT

We present high-angular (∼0.″4) resolution mid-infrared (MIR) polarimetric observations in the 8.7 μm and 11.6 μm filters of Cygnus A using CanariCam on the 10.4 m Gran Telescopio CANARIAS. A highly polarized nucleus is observed with a degree of polarization of 11% ± 3% and 12% ± 3% and a position angle of polarization of 27° ± 8° and 35° ± 8° in a 0.″38 (∼380 pc) aperture for each filter. The observed rising of the polarized flux density with increasing wavelength is consistent with synchrotron radiation from the parsec-scale jet close to the core of Cygnus A. Based on our polarization model, the synchrotron emission from the parsec-scale jet is estimated to be 14% and 17% of the total flux density in the 8.7 μm and 11.6 μm filters, respectively. A blackbody component with a characteristic temperature of 220 K accounts for >75% of the observed MIR total flux density. The blackbody emission arises from a combination of (1) dust emission in the torus; and (2) diffuse dust emission around the nuclear region, but the contributions of the two components cannot be well-constrained in these observations.

Key words: galaxies: active – galaxies: individual (Cygnus A) – infrared: galaxies – techniques: polarimetric

Online-only material: color figures

1. INTRODUCTION

Little is known about the mid-infrared (MIR) polarization at the high-angular resolution of active galactic nuclei (AGNs). The only high-angular resolution MIR polarimetric observations of an AGN were published by Packham et al. (2007), who used the polarimetric mode of MICHELLE with the 9.7 μm filter on the 8.1 m Gemini North telescope. This study revealed complex polarization structures in the inner 2″ of NGC 1068. However, only one filter was used, making a full interpretation of the different mechanisms of polarization difficult. The polarization mechanisms and hence the physical mechanisms and the nature of the inner region of the AGN can be disentangled only through multi-wavelength MIR polarimetric observations (Aitken et al. 2004).

At a redshift of 0.0562 (Stockton et al. (1994), H_0 = 73 km s^{-1} Mpc^{-1}; 1″ ∼ 1 kpc), Cygnus A is one of the most studied Faranoff–Riley class II (FRII) radio galaxies (Carilli & Barthel 1996). Cygnus A shows complex structures: including a core with a patchy dust lane, ionization cones, and jets. A compact, unresolved nucleus, with a peak in the luminosity at IR wavelengths was observed using the Palomar 5.08 m Hale Telescope (Djorgovski et al. 1991). Based on their reported visual extinction A_V = 50 ± 30 mag and the IR luminosity, Cygnus A should be classified as a quasar. The classification as a quasar has also been made by several others (e.g., Ueno et al. 1994; Tadhunter et al. 1999), with different estimations of the visual extinction to the nucleus of Cygnus A. For instance, Ueno et al. (1994) obtained a visual extinction of 170 ± 30 mag from modeling the X-ray spectrum. Simpson (1995) compared the [O III] emission lines, MIR continuum, and hard X-ray continuum and estimated a visual extinction of 143 ± 35 mag. Using high-spatial resolution *Hubble Space Telescope* (*HST*)/NICMOS observations in the 2.0 μm filter and the near-infrared (NIR) to X-ray correlation (Kriss 1988) for quasars, Tadhunter et al. (1999) estimated a visual extinction of 94 mag. The discrepancy between visual extinctions at different wavelengths can be accounted for as different wavelengths penetrate through different depths and structures in and around the central engine. The X-ray values represent the best estimate for the total extinction to the central engine of Cygnus A, while NIR values are dominated by emission line and/or hot (T ∼ 1000 K) dust emission close to the central engine. The MIR emission dominantly arises from warm (T ∼ 300 K) dust within the torus and/or dust emission from extended dust component.

Although optical total flux emission (as opposed to polarized flux emission) from the central engine is not observed, optical polarized broad emission lines have been observed (e.g., Tadhunter et al. 1990; Jackson & Tadhunter 1993; Ogle et al. 1997). This is most readily interpreted by the presence of broad emission lines in the central engine scattered into our line of sight (LOS), which would otherwise be obscured by the

[13] August G. Linares Senior Research Fellow.
[14] Marie Curie Fellow.

geometrically and optically thick and dusty torus. Such an interpretation is entirely consistent with the unified model of AGNs (Antonucci 1993; Urry & Padovani 1995). Also, it shows the potential of polarimetric techniques to investigate the core of Cygnus A. Previous studies (Tadhunter et al. 1990) observed, in the *V* band, a centrosymmetric polarization pattern along the ionization cones in the inner ∼3.″5 of Cygnus A. This polarization pattern is the signature of a central point source core whose radiation is polarized through scattering by dust and/or electrons. Jackson & Tadhunter (1993) observed an optical (0.48–0.78 μm) polarized spectrum rising to the blue, suggesting that dust scattering is the dominant mechanism of polarization responsible for the extended optical polarized flux of Cygnus A. Through spectropolarimetric observations in the range of 0.3–0.85 μm, Ogle et al. (1997) investigated the broad and narrow emission lines and the color and high polarization of the scattered continuum. They concluded that all features are consistent with scattering by dust. Thus, an extended dusty component is dominantly responsible for the polarized flux through dust scattering at optical wavelengths.

Further high-angular resolution *HST*/NICMOS observations, using the 1.1 μm, 1.6 μm, 2.0 μm and 2.25 μm filters, detailed the region of the AGN and the ionization cones (Tadhunter et al. 1999). This study detected an X-shape structure consistent with straight lines in the central 2″ of Cygnus A. This structure was also observed in 10.8 μm and 18.2 μm broad-filters imaging observations using OSCIR on the 10.0 m Keck II telescope (Radomski et al. 2002), as well as in 11.7 μm narrow-filter imaging observations using the long wavelength spectrometer (LWS) on the 10.0 m Keck I telescope (Whysong & Antonucci 2004). Imaging polarimetric observations in the 2.0 μm filter using *HST*/NICMOS detected highly polarized extended emission with a maximum in the degree of polarization of ∼25%, spatially coincident with one arm of the biconical structures seen in total flux (Tadhunter et al. 2000, hereafter T00). They suggested that scattering is the dominant polarizing mechanism in the 2.0 μm filter and that the detection of only one arm in polarized flux could be produced by intrinsic anisotropy from the central engine, possibly a warped disk.

Several studies have investigated the different components within the unresolved nucleus of Cygnus A using polarimetric techniques. In the 2.0 μm filter, T00 measured the nucleus to have a degree of polarization of ∼20% at the flux peak and ∼10% in a 0.″375 × 0.″375 aperture. This is most readily accounted for by an unresolved scattering region close to the central engine. However, as only a single wavelength was available, definitive conclusions about the polarization mechanisms could not be drawn. A kinematic study (van Bemmel et al. 2003) of the polarized [O III] emission lines showed that a dust scattering component arises from spatially unresolved optically thin dusty clouds moving away from the nucleus of Cygnus A and along the dusty biconical structures observed at NIR (Tadhunter et al. 1999) and MIR (Radomski et al. 2002; Whysong & Antonucci 2004) wavelengths. Although radio polarimetric observations of Cygnus A have not been published, parsec-scale jets have been observed (Krichbaum et al. 1998) through VLBI radio observations in Cygnus A, consistent with the classification as an FRII source and with the presence of a synchrotron component close to the AGN.

In total flux, recent studies (Privon et al. 2012; Merlo et al. 2014) have modeled the spectral energy distribution (SED) of the central regions of Cygnus A. Privon et al. (2012, hereafter P12) suggested that the SED can be explained by (1) star formation, dominant in the far-IR (FIR); (2) clumpy torus emission with a diameter of ∼130 pc, dominant in the MIR; and (3) a cut-off wavelength synchrotron component with a break in the MIR. Through high-angular resolution, *N*-band spectroscopic observations using the 8.2 m Subaru telescope, Merlo et al. (2014) suggested that the MIR total flux emission can be explained by a blackbody component of 217 ± 3 K located in our LOS to the AGN. To further investigate the MIR core of Cygnus A and examine the strength of the synchrotron jet, MIR polarimetry can be a powerful tool.

In this paper, we aim to explain the dominant mechanism of polarization of Cygnus A at MIR wavelengths. We present high-angular (∼0.″4) resolution polarimetric observations in the 8.7 μm and 11.6 μm filters using CanariCam on the 10.4 m Gran Telescopio CANARIAS (GTC). This paper is organized as follows. We describe the observations and data reduction in Section 2 and the results are presented in Section 3. A polarization model to account for the IR polarization of Cygnus A is presented in Section 4. Section 5 presents the discussion of our results and Section 6 presents the conclusions.

2. OBSERVATIONS AND DATA REDUCTION

Cygnus A was observed on 2012 August 12 during the commissioning of the imaging polarimetric mode (Packham et al. 2005) of CanariCam (Telesco et al. 2003) on the 10.4 m GTC in La Palma, Spain. CanariCam uses a Raytheon 320 × 240 pixels Si:As array, with a pixel scale of 0.″0798 pixel^{-1}. The polarimetric mode of CanariCam uses a half-wave plate (HWP), a field mask, and a Wollaston prism. The Wollaston prism and HWP are made from sulfur-free CdSe. The HWP has a chromatic dependency on the polarization retardation, resulting in a variable polarimetric efficiency across the wavelength range of 7.5–13 μm. However, this has been well-determined.[15] In standard polarimetric observations, the HWP is rotated in four position angles (P.A.) in the following sequence: 0°, 45°, 22.°5, and 67.°5. The field mask consists of a series of slots of 320 × 25 pixels each, corresponding to a field of view (FOV) of 25.″6 × 2.″0, where a total of three slots can be used, providing a non-contiguous total FOV of 25.″6 × 6.″0.

The Si2 ($\lambda_c = 8.7$ μm, $\Delta\lambda = 1.1$ μm, 50% cut-on/off) and Si5 ($\lambda_c = 11.6$ μm, $\Delta\lambda = 0.9$ μm, 50% cut-on/off) filters provide the best combination of sensitivity, spatial resolution, and spread in wavelength within the instrument filter set; thus, these filters were used for the observations. Observations were made using a standard chop–nod technique to remove time-variable sky background and telescope thermal emission, and to reduce the effect of $1/f$ noise from the array. In all observations, the chop throw was 8″, the chop angle was 105°E of N to locate the extended dust emission of Cygnus A along the FOV of the slot and the chop frequency was 1.93 Hz. The angle of the short axis of the array with respect to the north on the sky (i.e., instrumental P.A.) was 15°E of N and the telescope was nodded every 45.5s along the chopping direction. Only one slot with an FOV of 25.″6 × 2.″0 was used in these observations. In both filters, we took two sets of images with an on-source time of 582s each. To improve the signal-to-noise ratio (S/N) in the final image, the negative images (produced by the chop–nod technique) on the array were also used, providing a useful on-source time of 2328 s for each filter.

[15] Further information about the polarization efficiency is at http://www.gtc.iac.es/instruments/canaricam/∼#Polarization_Measurement_Efficiency.

Data were reduced using custom IDL routines. The difference for each chopped pair was calculated and the nod frames were then differenced and combined to create a single image per HWP P.A. During this process, all nods were examined for high and/or variable background that could indicate the presence of clouds or high precipitable water vapor, but no data needed to be removed for these reasons. Since Cygnus A was observed in two different sets of images, each HWP P.A. frame was registered and shifted to a common position, then images with the same HWP P.A. were coaveraged. Next, the ordinary (o-ray) and extraordinary (e-ray) rays, produced by the Wollaston prism, were extracted and Stokes parameters, I, Q, and U were estimated according to the ratio method prescription (e.g., Tinbergen 2006). Finally, the degree, $P = \sqrt{Q^2 + U^2}/I$, and P.A., P.A. $= 0.5 \arctan(U/Q)$, of polarization were estimated.

The polarized young stellar object, AFGL 2403, was observed in the 8.7 μm filter immediately before Cygnus A. In total flux, AFGL 2403 was used as a point-spread function (PSF) star, where the FWHM was 0.″38. A Moffat function with two parameters, FWHM and β parameter, best describes the delivered PSF (see Radomski et al. 2008). As seeing improves at longer wavelengths, and 0.″38 is much larger than the diffraction limit at 11.6 μm (∼0.″28), this can be considered to be a conservative FWHM for the 11.6 μm filter. In polarimetry, AFGL 2403 allowed us to estimate the zero-angle calibration of the observations. The zero-angle calibration, $\Delta\theta$, was estimated as the difference of the measured P.A. of our observations' polarization, $\theta = 54^\circ \pm 8^\circ$, and the P.A. of polarization measured by Smith et al. (2000), $\theta_s = 40^\circ \pm 8^\circ$. Thus, the zero-angle calibration was estimated to be $\Delta\theta = \theta_s - \theta = -14^\circ$. Our measured degree of polarization, 1.6% ± 0.5%, of AFGL 2403 was in excellent agreement with the measured degree of polarization, 1.5% ± 0.4%, by Smith et al. (2000).

The instrumental polarization was corrected based on data provided by the GTC Web site.[16] Specifically, the instrumental polarization is $P_{\rm ins} = 0.5\% \pm 0.2\%$ in all filters with a dependency in the P.A. of polarization given by P.A.$_{\rm ins} = -$(RMA+Elev) $-$ 29.°6, where RMA is the Nasmyth rotator mechanical angle and Elev is the telescope elevation. The instrumental polarization was corrected as follow. The normalized Stokes parameters, $q_{\rm ins} = Q_{\rm ins}/I_{\rm ins}$ and $u_{\rm ins} = U_{\rm ins}/I_{\rm ins}$, of the instrumental polarization were estimated using the degree, $P_{\rm ins}$, and position angle, P.A.$_{\rm ins}$, of the instrumental polarization. Then, the q$_{\rm ins}$ and u$_{\rm ins}$ were subtracted from the normalized Stokes parameters of Cygnus A.

Dedicated flux standard stars were not observed. Flux calibration was performed using the 8–13 μm spectrum acquired in a 0.″5 slit with the LWS on the 10.0 m Keck I telescope by Imanishi & Ueno (2000). The flux densities from the MIR spectra of Cygnus A are 50 ± 10 mJy and 110 ± 22 mJy at 8.7 μm and 11.6 μm, respectively. Then, measured counts in a 0.″5 × 0.″5 simulated slit aperture from our images in the 8.7 μm and 11.6 μm filters were equated to the flux densities from the MIR spectra by Imanishi & Ueno (2000). Finally, the factor mJy counts^{-1} was estimated and used in the measurements of the flux densities in the several apertures presented in Section 3. As the dominant contributor to the uncertainty in the measurements of the total flux densities is based on the calibration from MIR spectroscopic data using Keck I by Imanishi & Ueno (2000), we used the uncertainty of 20% for the measurements of the total flux densities in our observations.

[16] Further information about the instrumental polarization of CanariCam can be found at http://www.gtc.iac.es/instruments/canaricam/#Instrumental_Polarization.

Table 1
Aperture Flux Density and Polarization Measurements

Filter	Aperture Diameter (″)	Flux Density (mJy)	P (%)	P.A. (°)
8.7 μm[a]	0.38	29 ± 6	11 ± 3	27 ± 8
	2.0	101 ± 20	···	···
11.6 μm[a]	0.38	45 ± 9	12 ± 3	35 ± 8
	2.0	169 ± 34	···	···
2.0 μm[b]	0.375	4.9 ± 0.1	10 ± 1.5	201 ± 3
N band[c]	2.0	104 ± 3	···	···
11.7 μm[d]	1.92	122 ± 12	···	···

References. (a) This work; (b) Tadhunter et al. 2000; (c) Radomski et al. 2002; (d) Whysong & Antonucci 2004

3. RESULTS

We made measurements of the nuclear flux density in several apertures to compare with previously published values (Table 1). We measured the aperture flux density to be 29 ± 6 mJy and 45 ± 9 mJy in the 8.7 μm and 11.6 μm filters, respectively, in an aperture diameter (hereafter aperture refers to diameter) equal to the FWHM, 0.″38 (∼380 pc), of the PSF. This value optimally measures the nuclear flux density of Cygnus A and minimizes contamination from extended (diffuse) warm nuclear and emission from heated dust. The statistical significance of the aperture flux detections is ∼40σ in both filters.

We measured the nuclear polarization using the I, Q, and U images in a 0.″38 aperture, to match the FWHM of the observations. The degree of polarization was measured to be 11% ± 3% and 12% ± 3% with a P.A. of polarization measured to be 27° ± 8° and 35° ± 8° in the 8.7 μm and 11.6 μm filters, respectively. The statistical significance of the polarization measurements is ∼4σ of the polarization degree in both filters. The uncertainties in the degree of polarization and P.A. of polarization were estimated using the method of Naghizadeh-Khouei & Clarke (1993), which estimates the uncertainties based on the S/N and measured degree and P.A. of polarization values.

Figure 1 shows the total flux images in the 8.7 μm and 11.6 μm filters with the lowest contour at the 5σ level. Due to the low S/N of the polarization detection, the polarization measurement is treated as a single statistically significant polarization vector at the 4σ level of the polarization degree using the 0.″38 aperture in the 8.7 μm and 11.6 μm filters (Table 1). In total flux, the images in the 8.7 μm and 11.6 μm filters show a point source at the position of the nucleus with diffuse dust emission around the nuclear region with two extended emissions along the NE and SE arms of the ionization cones, previously observed in the 10.8 μm broad-filter imaging (Radomski et al. 2002) and in the 11.7 μm narrow-filter imaging (Whysong & Antonucci 2004). In our 11.6 μm filter observations, we detect diffuse extended dust emission in the NW arm at the 5σ level in total flux. This diffuse extended dust emission component is spatially coincident with the extension previously observed in the 2.0 μm filter using *HST*/NICMOS by Tadhunter et al. (1999).

Previous NIR polarization measurements found a perpendicular P.A. of polarization with the radio jet in Cygnus A. Specifically, T00 measured a nuclear P.A. of polarization in

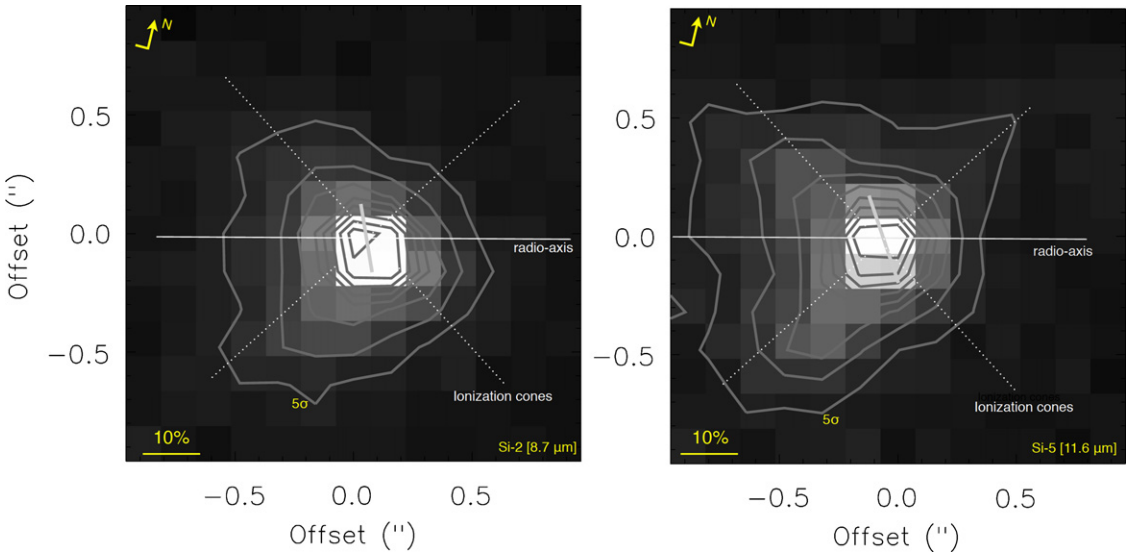

Figure 1. Total flux (grayscale) images and nuclear polarization vector in a 0.″38 (∼380 pc) aperture of Cygnus A in the 8.7 μm (left) and 11.6 μm (right) filters. Contours start at 5σ and increase in steps of 5σ. A polarization vector of 10% polarization is shown (bottom left). Total flux images were binned using a 2 × 2 pixel (0.″16 × 0.″16) box only for display purposes. Radio axis (solid line) with P.A.$_{\rm jet}$ = 284° ± 5° (Sorathia et al. 1996) and ionization cones (dashed line; Tadhunter et al. 1999) are shown.

(A color version of this figure is available in the online journal.)

the 2 μm filter of P.A.$_{2\mu{\rm m}}$ = 201° ± 3°, almost perpendicular (83° ± 6°) to the radio jet axis, P.A.$_{\rm jet}$ = 284° ± 5° (Sorathia et al. 1996).We find that the MIR P.A. of polarization is rotated by 77° ± 13°and 69° ± 13°in the 8.7 μm and 11.6 μm filters from the P.A.$_{\rm jet}$. In common with the 2.0 μm observations, this is close to perpendicular to the P.A.$_{\rm jet}$. The estimation of the rotations are not exactly perpendicular to the radio jet axis, which can be attributed to (1) the relatively large uncertainty in the P.A. of polarization due to low S/N; and (2) the possible mix of several mechanisms of polarization (Sections 4 and 5) as well as different dominant polarization mechanisms at different wavelengths within the 0.″38 aperture.

4. POLARIZATION MODEL

We aim to reproduce the observed polarization from 2.0 μm to 11.6 μm. Specifically, we need a polarization component that reproduces the observed polarized flux rising with increasing wavelength. We developed a polarization model that simultaneously fits the total flux, degree of polarization, and polarized flux. In the model, we consider the following components: (1) stellar emission from the nuclear bulge, (2) extinguished AGN emission, (3) scattered radiation by dust within the unresolved nuclear region, (4) thermal emission from dust (torus and/or diffuse dust emission), and (5) synchrotron radiation from the parsec-scale jet. To constrain the polarization mechanisms, we used our polarimetric measurements in a 0.″38 aperture in the 8.7 μm and 11.6 μm filters (Table 1), in combination with the measured degree of polarization in the 2.0 μm filter of 10% ± 1.5% by T00. This measurement has similar aperture size to our MIR measurements and minimizes contamination from extended components and starlight.

Starlight emission and its possible polarization are negligible at 8.7 μm and 11.6 μm. T00 estimated the contribution of the AGN emission to be 35% at 2.0 μm through PSF subtraction and we assume that the stellar component is 65% of the total flux density. We use the 2.0 μm flux density data to estimate the flux density in our MIR filters, using a simple and approximate color correction of the total flux density in K (2.2 μm) to *N* band (10 μm), $S_{\rm N} = 0.091 S_{\rm K}$ (Knapp et al. 1992). This yields a flux density of 0.3 mJy in our 0.″38 aperture in the *N* band, which is ∼1% of the aperture flux density at 8.7 μm and a dichroic polarization of 0.1% (Serkowski et al. 1975). Both aperture flux density and dichroic polarization, are lower at 11.6 μm. Thus, the dichroic absorption of starlight is considered to be negligible given the high measured degree of polarization of Cygnus A within the 2–11.6 μm wavelength range.

The AGN emission, defined as the emission from the accretion disk of the central engine, is assumed to be an extinguished unpolarized power law, $F_\lambda \propto \lambda^{-\alpha_{\rm AGN}} e^{-\tau_\lambda}$, where τ_λ, is the absorption produced by the dust screen (i.e., dust lane). We adopted a spectral index $\alpha_{\rm AGN} = 1.8$ from the intrinsic infrared AGN SED template in the wavelength range of 6–19 μm (Mullaney et al. 2011). As in the case of the bulge component, this simple AGN power law ensures no additional free parameters, silicate features and/or uncertainties in the polarization model. Recent studies have demonstrated that a "universal" NIR to MIR extinction law cannot be defined (e.g., Fitzpatrick & Massa 2009; Gao et al. 2009). However, the standard silicate–graphite interstellar grain for $R_{\rm v} = 5.5$ appears to be in agreement with the MIR extinction curves at different sightlines through the Galactic center (Weingartner & Draine 2001). We took the extinction law[17] for $R_{\rm v} = 5.5$, with $A_{8.7\,\mu{\rm m}} \sim A_{11.6\,\mu{\rm m}} = 0.75\,A_{\rm K}$ (Figure 1 in Gao et al. 2013), and $A_{\rm K} = 0.112\,A_{\rm V}$ (Jones 1989). We took the visual extinction of $A_{\rm v} = 94$ mag to the nucleus of Cygnus A (Tadhunter et al. 1999), because it represents the most comparable value to our aperture size and wavelength.

As noted in the introduction, dust scattering is the dominant polarization mechanism in the central regions of Cygnus A at optical wavelengths (Tadhunter et al. 1990; Jackson & Tadhunter 1993; Ogle et al. 1997; van Bemmel et al. 2003). To study how dust scattering affects polarization in the unresolved nucleus of Cygnus A within the 2–11.6 μm wavelength range, this mechanism is included in our polarization model. We

[17] Note that recent studies (Gao et al. 2013) suggested that a trimodal grain-size distribution with a combination of $R_{\rm v} = 2.1$, 3.1, and 5.5 is required to achieve a good fit to the extinction curve from the UV to the MIR.

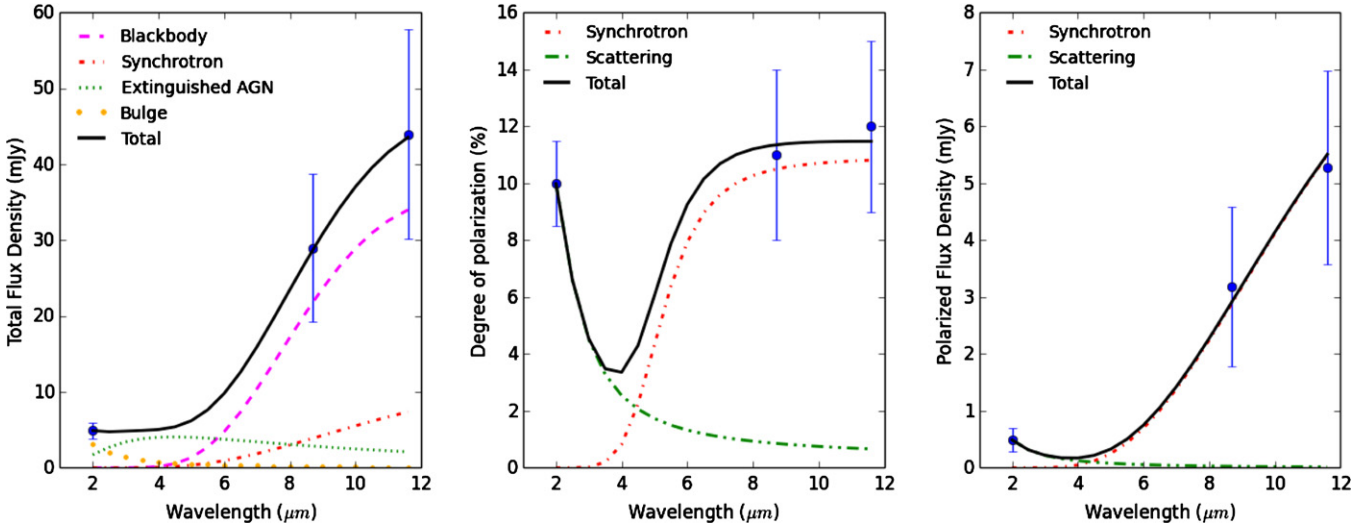

Figure 2. Model fit to the measured total flux density (left panel) in a 0.″38 (∼380 pc) aperture is shown. Measured total flux density (blue dots), nuclear bulge (orange circles), extinguished AGN emission (green dots), synchrotron radiation from the parsec-scale jet (red dash-dotted), blackbody emission at 220 K (magenta dashed), and the total model (black solid) are shown. Model fit to the measured degree of polarization (middle panel) and polarized flux density (right panel) in a 0.″38 (∼380 pc) aperture are shown. Measured degree of polarization (blue dots), measured polarized flux density (blue dots), synchrotron radiation from the parsec-scale jet (red dashed–dotted–dotted), dust scattering (green dash-dotted) and total model (black solid) are shown.

(A color version of this figure is available in the online journal.)

assumed a wavelength dependency in the total flux density to be $F^{\rm sca} \propto \lambda^{-4}$, consistent with scattered radiation by dust within the unresolved core. The degree of polarization is also a function of the wavelength, $P^{\rm sca} \propto \lambda^{-4}$. We took the intrinsic degree of polarization of 28% estimated by T00 at 2.0 μm, to estimate the observed polarization in our polarization model.

For MIR thermal emission in the core of Cygnus A, Radomski et al. (2002) estimated that temperature reaches a value of 150 ± 10 K up to 500 pc from the central source, with a lower limit of 220 ± 30 K in the NE cone and 150 ± 5 K in the SE cone. Whysong & Antonucci (2004) estimated a temperature of 120 K up to 500 pc from the core of Cygnus A. Merlo et al. (2014) suggested that the MIR emission is produced by a blackbody component with a characteristic temperature of 217 ± 3 K in our LOS to the core. Based on these studies and the physical size (∼380 pc) of our aperture, the final characteristic temperature of the blackbody component in our polarization model was estimated as the best fit of a blackbody component in steps of 10 K within the range of 120–220 K. We assume this blackbody component arises from the diffuse dust emission around the nuclear region and/or dusty torus. This component is assumed to be unpolarized and no dichroism is considered in the polarization model (Section 5).

As noted in the introduction, previous studies have observed parsec-scaled jets that contribute, at some fraction, to the total flux density as a synchrotron component with a cut-off wavelength in the MIR wavelengths. In our model, synchrotron emission is described as a cut-off wavelength power-law source behind a dust screen (i.e., dust lane), $F_\nu^{\rm syn} \propto e^{-\nu/\nu_c}\nu^{-\alpha_{\rm syn}}e^{-\tau_\lambda}$, where ν_c, is the cut-off frequency; $\alpha_{\rm syn}$, is the spectral index; and τ_λ, is the absorption produced by the dust screen. We took the spectral index, $\alpha_{\rm syn}$, of 0.18 estimated using radio Very Long Baseline Array (VLBA) observations and previously used in the SED models by P12. Recent polarimetric studies(Ramirez et al. 2014) in the 2.0 μm filter using *HST*/NICMOS, in combination with radio and millimeter wavelengths, of a sample of narrow-line radio galaxies (Cygnus A included) estimated an averaged spectral index of 0.21 ± 0.1 (0.18 for Cygnus A). The parsec-scale jet has been resolved using VLBA observations (Sorathia et al. 1996), hence the only extinction along our LOS to be considered is that produced by the dust lane of the Cygnus A galaxy. We took the visual extinction of the dust lane of 5.5 mag as modeled by Packham et al. (1998). The polarized flux density of the synchrotron radiation follows the same power-law source as the total flux density.

Table 2
Fraction of Aperture and Polarized Flux Density for Each Mechanism in the Central 380 pc of Cygnus A

Component	2.0 μm	8.7 μm	11.6 μm
		Total Flux Density	
Nuclear bulge	65%	Negligible	Negligible
Extinguished AGN	35%	10%	5%
Synchrotron	Negligible	14%	17%
Blackbody radiation	Negligible	75%	78%
		Polarized Flux Density	
Dust scattering	>99%	Negligible	Negligible
Synchrotron	Negligible	>99%	>99%

With the constraints on each component given above, we simultaneously fit the measured total flux density, degree of polarization, and polarized flux (Figure 2). The fit was considered acceptable when the deviations from the modeled total and polarized flux values were <5% of the measured values at 2.0 μm, 8.7 μm and 11.6 μm. For the best fit, we found a blackbody component with a characteristic temperature of 220 K and a synchrotron cut-off wavelength at 34 μm. Within an aperture of 0.″38 (∼380 pc), the fraction of total and polarized flux density for each one of the components in our polarization model are shown in Table 2. Note that this polarization model is excluding polarization from dichroic emission, which can contribute at a low level to the total polarized flux density.

5. DISCUSSION

The most plausible explanation of the polarization in the nucleus of Cygnus A is that the MIR polarization dominantly arises from synchrotron radiation. The intrinsically polarized source

flux is diluted by the blackbody component with a characteristic temperature of 220 K. The intrinsic polarization is estimated to be $P_{syn}^{int} \sim 65\%$ in the MIR wavelengths. This value is in agreement with a linear polarization as high as 70% produced by optically thin synchrotron radiation. The high intrinsic degree of polarization implies a very ordered magnetic field within the parsec-scale jet close to the core of Cygnus A. This characteristic has been previously observed in Cygnus A (Krichbaum et al. 1998) and other AGNs, e.g., NGC 1052 (Vermeulen et al. 2003). Also, shock waves within the jets compress the magnetic field and create regions of ordered magnetic fields (Laing 1980). A high intrinsic polarization with the P.A. of polarization approximately perpendicular to the parsec-scale jet are readily produced by synchrotron radiation from the parsec-scale jet observed at radio wavelengths (Krichbaum et al. 1998). The P.A. of polarization is coincident for both the NIR and MIR wavelengths. The P.A. of polarization arising from scattering within the innermost region of the central engine of Cygnus A will be aligned with the major axis of the torus, i.e., perpendicular to the polar axis. This implies that the P.A. of polarization in the NIR and MIR will be nearly the same, but that the dominant mechanisms of polarization are not the same.

The polarization model explains the observed MIR total flux density from the contribution of (1) a blackbody component with a characteristic temperature of 220 K and (2) a synchrotron component. The latter only contributes 14% and 17% of the observed nuclear total flux density in the 8.7 μm and 11.6 μm filters, respectively (Table 2). From our polarization model, the blackbody emission with a characteristic temperature of 220 K can arise from (1) dust in the torus and/or (2) a diffuse dust emission component in our LOS. The temperature is consistent with directly radiated dust from the central engine located at a radius of $\sim$130 pc, as well as emitted radiation from dust in the non-directly illuminated faces of the clumps within the torus at scales of few parsecs from the central engine. Thus, these components cannot be distinguished from the current model.

Several NIR polarimetric studies (e.g., Jones & Klebe 1989; Young et al. 1995; Packham et al. 1998; Simpson et al. 2002) of AGNs have found that some of the nuclear polarization of type 2 AGNs often arises from the passage of unpolarized radiation from the central engine through aligned dust grains in the torus in our LOS. To investigate the effect that this mechanism could have on our observations, we investigate it here. Jones et al. (1992) explained the trend of polarization with optical depth in the interstellar medium (ISM) using grains aligned with a magnetic field, which was a mixture of constant and random components. If the visual extinction of 94 mag (Tadhunter et al. 1999) to the nucleus of Cygnus A is assumed, the predicted level of polarization at K produced by dichroic absorption is 51% for a constant component of the magnetic field, 3% for random alignment of the magnetic field, and 11% for equal contribution of the constant and random component of the magnetic field. If we assume that the intrinsic polarization in the 2.0 μm filter of 28% (T00) arises from dichroic absorption of unpolarized radiation of the central engine by aligned dust grains in our LOS, then Cygnus A has a constant component of the magnetic field dominating the thermal motions in determining the alignment geometry of dust grains. Although some dust grain alignment (though far from perfect alignment) is expected, it is difficult to distinguish where the dichroic absorption arises: (1) within the torus or (2) from the dusty blackbody component in our LOS. We believe that, in agreement with T00, such a high, 28%, intrinsic degree of polarization at 2.0 μm is far more likely to arise from a scattering region close to the central engine of Cygnus A rather than dichroism. Furthermore, we note that such a high level of intrinsic of polarization produced by dichroism is rarely observed in other AGNs at NIR wavelengths (e.g., Lopez-Rodriguez et al. 2013; Ramirez et al. 2014). Thus, although we cannot exclude the possibility of a dichroic absorption source of the polarization, we find it very unlikely.

Vernet et al. (2001) showed that the UV–optical continuum of several quasars at $z \sim 2.5$ can be explained by dust-reflected quasar light resulting in gray scattering (large dust grains produce scattering with a constant degree of polarization) from a highly clumped scattering medium close to the nucleus. We studied the possibility of large grains in a clumped medium close to the core of Cygnus A. This clumped medium produces a gray scattering component, reddened by the blackbody component in our LOS, which can explain the polarized flux density rising with increasing wavelength. Large grains are considered when grain sizes are the order of the incident radiation wavelength. In this case, grain sizes of $\sim$1 μm and $\sim$10 μm from NIR and MIR radiation, respectively, are required. These grain sizes are very difficult to conceive with typical ISM dust grains, where typical grain models (Mathis et al. 1977) suggest grain sizes between 0.005–0.25 μm. Although the observed polarized flux density rising with wavelength in Cygnus A (Figure 2) can be fit by a gray scattering model, this mechanism is difficult to conceive given the large grain sizes that are required to fit the data.

6. CONCLUSIONS

We found that synchrotron radiation from a parsec-scale jet close to the core of Cygnus A is the most likely mechanism to explain the polarized flux rising with increasing wavelength. Based on our developed polarization model, the synchrotron radiation from the parsec-scale jet is estimated to be 14% and 17% of the total flux density in the 8.7 μm and 11.6 μm filters, respectively. A blackbody component with a characteristic temperature of 220 K can account for >75% of the observed MIR total flux density. The blackbody emission can arise from (1) dust in the torus and/or (2) a diffuse dust emission component in our LOS, but these two components cannot be distinguished from the current observations. These observations represent the most compelling detection of a synchrotron component using MIR polarimetric observations in Cygnus A. Similar future observations of a sample of radio galaxies will be interesting to determine general and/or extraordinary properties in these objects.

We thank the anonymous referee for useful comments which significantly improved the paper. This work is based on observations made with the Gran Telescopio CANARIAS, installed in the Spanish Observatorio del Roque de los Muchachos of the Instituto de Astrofísica de Canarias, in the island of La Palma. E.L.R. acknowledges support from the University of Florida Alumni Fellowship for making this work possible as part of his thesis project, and also acknowledges the financial support of the University of Texas at San Antonio. C.P. acknowledges support from NSF-0904421 grant. A.A.H. acknowledges support from the Spanish Plan Nacional through grant AYA2009-05705-E. C.R.A. acknowledges support from the Marie Curie Intra European Fellowship PIEF-GA-2012-327934 within the 7th European Community Framework Programme and from the Spanish Plan Nacional through grant AYA2010-21887-C04.04

(Estallidos). R.M. and N.A.L. are supported by the Gemini Observatory, which is operated by the Association of Universities for Research in Astronomy, Inc., on behalf of the international Gemini partnership of Argentina, Australia, Brazil, Canada, Chile, and the United States of America. E.P. acknowledges support from AST-0904896.

REFERENCES

Aitken, D. K., Hough, J. H., Roche, P. F., Smith, C. H., & Wright, C. M. 2004, MNRAS, 348, 279
Antonucci, R. J. 1993, ARA&A, 31, 473
Carilli, C. L., & Barthel, P. D. 1996, A&ARv, 7, 1
Djorgovski, S., Weir, N., Matthews, K., & Graham, J. R. 1991, ApJL, 372, L67
Fitzpatrick, E. L., & Massa, D. 2009, ApJ, 699, 1209
Gao, J., Jiang, B. W., & Li, A. 2009, ApJ, 707, 89
Gao, J., Li, A., & Jian, B. W. 2013, EP&S, 65, 1127
Imanishi, M., & Ueno, S. 2000, ApJ, 535, 626
Jackson, N., & Tadhunter, C. N. 1993, A&A, 272, 105
Jones, T. J. 1989, ApJ, 346, 728
Jones, T. J., & Klebe, D. 1989, ApJ, 341, 707
Jones, T. J., Klebe, D., & Dickey, J. M. 1992, ApJ, 389, 602
Knapp, G. R., Gunn, J. E., & Wynn-Williams, C. G. 1992, ApJ, 399, 76
Krichbaum, T. P., Alef, W., Witzel, A., et al. 1998, A&A, 329, 873
Kriss, G. 1988, ApJ, 324, 809
Laing, R. A. 1980, MNRAS, 190, 439
Lopez-Rodriguez, E., Packham, C., Young, S., et al. 2013, MNRAS, 431, 2723
Mathis, J. S., Rumpl, W., & Nordsieck, K. H. 1977, ApJ, 217, 425
Merlo, M., Perlman, E., Packham, C., et al. 2014, ApJ, 788, 6
Mullaney, J. R., Alexander, D. M., Goulding, A. D., & Hickox, R. C. 2011, MNRAS, 414, 1082
Naghizadeh-Khouei, J., & Clarke, D. 1993, A&A, 274, 968
Ogle, P. M., Cohen, M., Miller, J. S., et al. 1997, ApJL, 482, L37
Packham, C., Hough, J. H., & Telesco, C. M. 2005, in ASP Conf. Ser. 343, CanariCam-Polarimetry: A Dual-Beam 10 microns Polarimeter for the GTC, ed. A. Adamson et al. (San Francisco, CA: ASP), 38
Packham, C., Young, S., Fisher, S., et al. 2007, ApJ, 661, 29
Packham, C., Young, S., Hough, J. H., Tadhunter, C. N., & Axon, D. J. 1998, MNRAS, 297, 936
Privon, G. C., Baum, S. A., O'Dea, C. P., et al. 2012, ApJ, 747, 46
Radomski, J. T., Packham, C., Levenson, N. A., et al. 2008, ApJ, 681, 141
Radomski, J. T., Piña, R. K., Packham, C., Telesco, C. M., & Tadhunter, C. N. 2002, ApJ, 566, 675
Ramirez, E. A., Tadhunter, C. N., Axon, D., et al. 2014, MNRAS, 444, 466
Serkowski, K., Mathewson, D. S., & Ford, V. L. 1975, ApJ, 196, 261
Simpson, C. 1995, PhD thesis, Univ. Oxford
Simpson, J. P., Colgan, S. J., Erickson, E. F., et al. 2002, ApJ, 574, 95
Smith, C. H., Wright, C. M., Aitken, D. K., Roche, P. F., & Hough, J. H. 2000, MNRAS, 312, 327
Sorathia, B., Barthel, N., Beitenholz, M., & Carilli, C. 1996, The parsec-scale jet and counter jet in Cygnus A (Cambridge: Cambridge Univ. Press)
Stockton, A., Ridgway, A., & Lilly, S. J. 1994, AJ, 108, 414
Tadhunter, C. N., Packham, C., Axon, D. J., et al. 1999, ApJL, 512, L91
Tadhunter, C. N., Scarrott, S. M., & Rolph, C. D. 1990, MNRAS, 246, 163
Tadhunter, C. N., Sparks, W., Axon, D. J., et al. 2000, MNRAS, 313, L52
Telesco, C. M., Ciardi, D., French, J., et al. 2003, Proc. SPIE, 4841, 913
Tinbergen, J. 2006, Astronomical Polarimetry (Cambridge: Cambridge Univ. Press)
Ueno, S., Koyama, K., Nishida, M., Yamauchi, S., & Ward, M. J. 1994, ApJL, 431, L1
Urry, C. M., & Padovani, P. 1995, PASP, 107, 803
van Bemmel, I. M., Vernet, J., Fosbury, R. A. E., & Lamers, H. G. L. M. 2003, MNRAS, 345, L13
Vernet, J., Forbury, R. A. E., Villar-Mart'n, M., et al. 2001, A&A, 366, 7
Vermeulen, R. C., Ros, E., Kellermann, K. I., et al. 2003, A&A, 401, 113
Weingartner, J., & Draine, B. T. 2001, ApJ, 548, 296
Whysong, D., & Antonucci, R. 2004, ApJ, 602, 116
Young, S., Hough, J. H., Axon, D. J., Bailey, J. A., & Ward, M. J. 1995, MNRAS, 272, 513